EUROPEAN ORGANIZATION FOR NUCLEAR RESEARCH
CERN — AB DEPARTMENT

CERN-AB-2006-083 BI

Status of the design of a Wide Band beam Current Monitor (WBCM) for EUROTeV

F. Caspers, R. Fandos, E. Jensen, T. Kroyer, I. Podadera Aliseda, L. Soby, I. Syratchev

CERN – Geneva - Switzerland

Abstract

In the framework of EUROTeV, the conceptual design of a new wide band wall current monitor is being carried out. The design is based on the wall current monitors presently installed in CTF3. The new design aims to increase the bandwidth up to 20 GHz. The present device has been tested in a dedicated test bench to understand its limitations in terms of bandwidth. The tests with the present device and the results of the conceptual design for the new one are summarized and discussed in this report.

Geneva, Switzerland
November, 2006

Status of the design of a Wide Band beam Current Monitor (WBCM) for EUROTeV

L. Soby, I. Podadera Aliseda, T. Kroyer, R. Fandos, I. Syratchev, F. Caspers, E. Jensen*

October 23, 2006

Abstract

In the framework of EUROTeV, the conceptual design of a new wide band wall current monitor is being carried out. The design is based on the wall current monitors presently installed in CTF3. The new design aims to increase the bandwidth up to 20 GHz. The present device has been tested in a dedicated test bench to understand its limitations in terms of bandwidth. The tests with the present device and the results of the conceptual design for the new one are summarized and discussed in this report.

*CERN, AB department, CH-1211 Geneva 23, Switzerland

1 Introduction

The new Wideband Beam Current Monitor (WBCM) is devoted to applications in future linear colliders (e.g. CLIC and ILC). For example, at CLIC [1] the new WCM will be in charge of providing essential information about the quality of the bunch combination after the combiner ring, where the bunch repetition frequency will be 15 GHz.

2 The existing design

The present Wall Current Monitor (WCM) is installed in the CTF3 facility [2]. Figure 1 shows a longitudinal cross section of that design. It is based on a previous design for the CTF2 facility [3]. The same concept has been used worldwide for many years, see [4, 5, 6]. Both versions are designed for a frequency bandwidth up to 10 GHz. They differ in two main points:

- Due to the longer pulse duration, the CTF3 version has a bigger inductance (bigger ferrite volume) to reduce the low frequency cut-off to 10 kHz.
- The miniature feedthroughs were modified in order to extend their bandwidth beyond 20 GHz [7].

In both versions, time domain measurements showed that the bandwidth is not as high as expected. Figure 2 shows the time domain measurement of the pulse response of the WCM prototype for the CTF3 (from [2]). The upper trace is the pulse at the input of the test bench ($FWHM = 24.5$ ps) and the lower trace is the WCM response measured on a 20 GHz oscilloscope after 1 m long cable ($FWHM = 55$ ps). Assuming gaussian input and output signals, the high frequency cut-off of the device f_{HC} (-3 dB or $1/\sqrt{2}$ of the maximum signal) is given by the expression:

$$f_{HC} \simeq \frac{0.32}{\sqrt{FWHM_{t2}^2 - FWHM_{t1}^2}}, \tag{1}$$

where $FWHM_{t1}$ and $FWHM_{t2}$ is the time full width at half maximum for the input and ouput signals, respectively. Therefore in this case, $f_{HC} \simeq 6.4$ GHz.

2.1 Measurements in frequency domain

A radio frequency network analyzer was used to carry out measurements in the frequency domain. The wire method was used for the measurements [8]. As sketched in the top of Fig. 3, the beam is simulated by using a cylindrical rod coaxial with the Device Under Test (DUT) in a 50 Ω environment. The results with the DUT are then compared with those obtained by substituting the DUT by a straight beam pipe (*reference*).
The measurements are summed up in Fig. 3. The measurement of the set-up without the DUT (reference) showed that, for frequencies above 4 GHz, the set-up does not work very well. There is a high reflection ($S_{11} > -10$ dB) above 4 GHz and low transmission

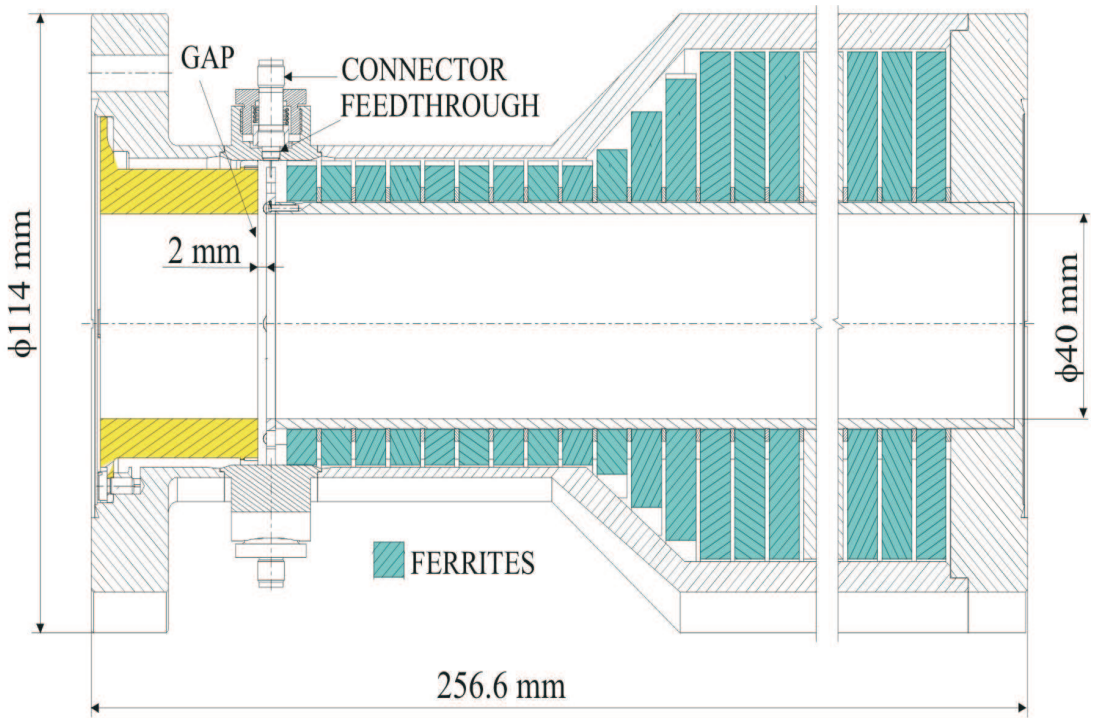

Figure 1: Longitudinal cross section of the WCM design for the CTF3 facility.

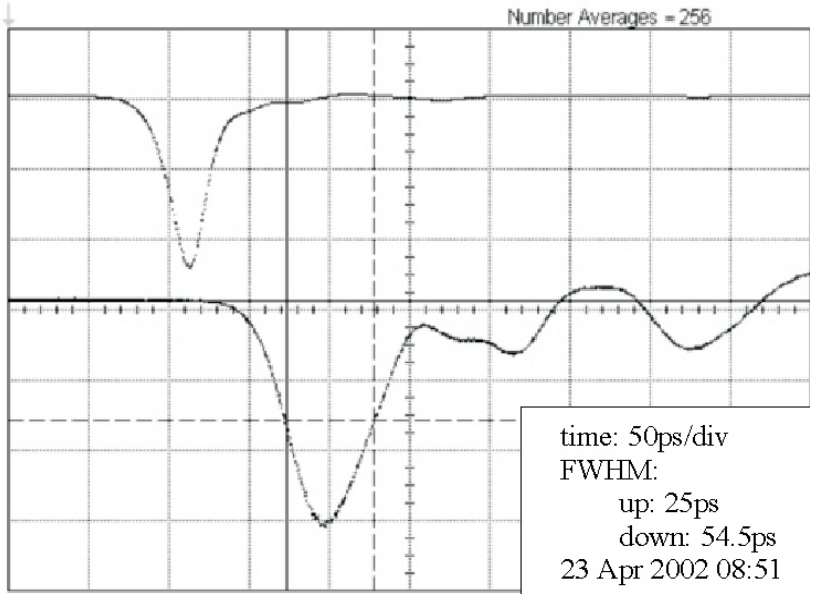

Figure 2: Measured pulse response of the prototype of the CTF3 WCM (from [2]).

($S_{21} < -3$ dB). The similarities of the transmissions measured with the DUT and with the reference implies that the resonances and ringings of both signals could come from Higher Order Modes (HOM's) appearing in the beam pipe ($TM_{01} = 5.7$ GHz, $TM_{02} = 13.2$ GHz and $TM_{03} = 20.7$ GHz). Further measurements with an improved test bench should be carried out in order to verify these points.
The pick-up signals were compared before (S_{311}) and after (S_{31}) the combination of the signal from the 8 feedthroughs [2]. The signal after the combiner is slightly lower and no resonances or signal degradation have been detected due to the signal combination.

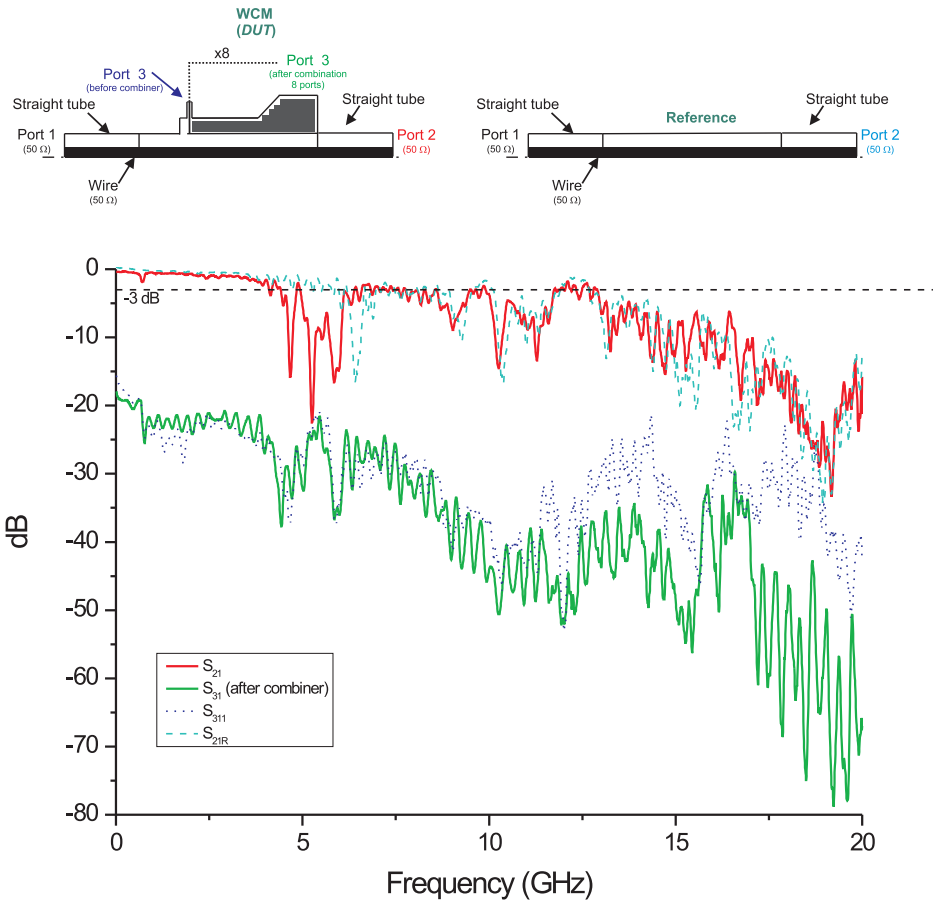

Figure 3: Plot of the measured S-parameters of the existing WCM: transmission of the WCM (S_{21}) and pick-up signals before (S_{311}) and after (S_{31}) signal combination. The transmission of the reference signal (S_{21R}) is also shown. The scheme of the measurements with the DUT and the reference is sketched on the top.

2.2 Simulations in frequency domain

Some frequency simulations using the wire method were carried out so as to try to detect the source of the limitation in the bandwidth for the existing CTF3 WCM version. The geometry input used for the HFSS code is shown in Fig. 4. Two variations are presented: 1) with a stack of ferrites, 2) solid ferrite in all the volume. No significant differences were found between both solutions. Therefore, because of its simplicity, the second geometry was used for all the simulations. The figure also shows the model of the ideal electrical vacuum feedthrough which guides to the external load, i.e. the signal combiner. In HFSS, the feedthrough is modeled using a 50 Ω coaxial structure. Because of computing limitations, only a small slice of the azimuthal symmetrical geometry is simulated, scaling the impedance of all the ports accordingly.

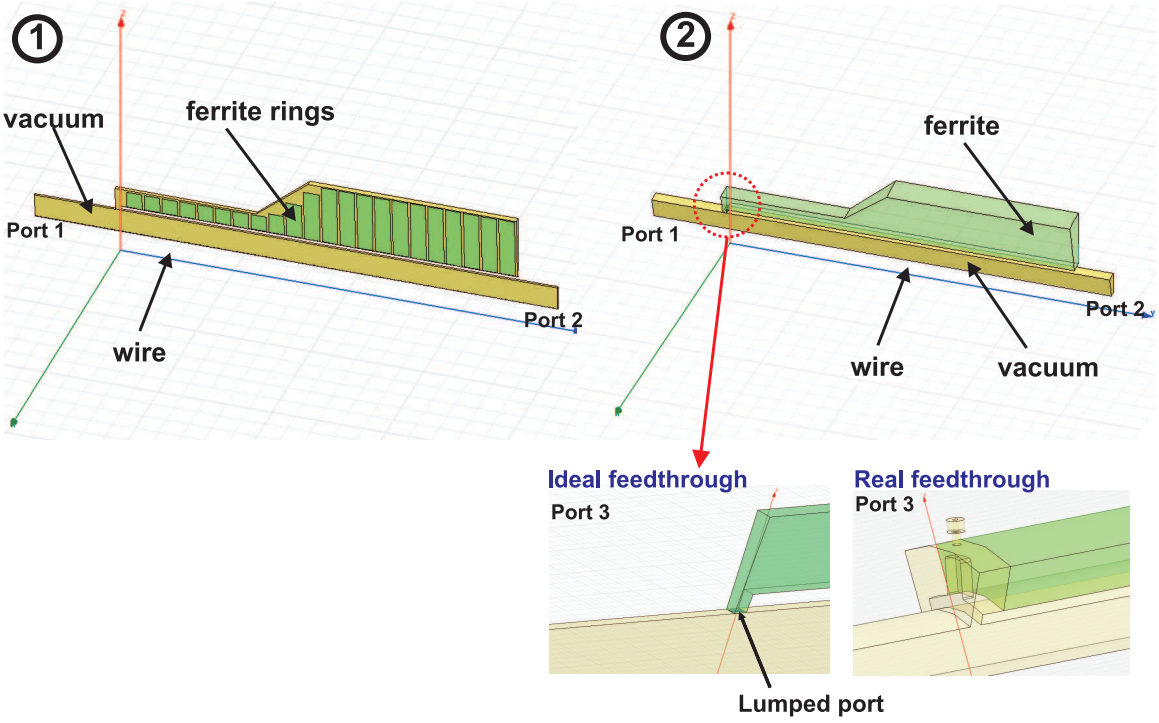

Figure 4: Geometry model used as input for the HFSS program: 1) with stack of ferrites, 2) solid ferrite model. The model for the ideal and the real feedthrough (more details later on the text) which pick up the signals are also shown.

2.2.1 Low frequency

To obtain good results at low frequencies it is essential to know the behavior of the ferrite material in this frequency range. The ferrite used is from the Fair-Rite company with quality number 61 [9]. The permeability of this material (μ' and μ") is only given up to 1 GHz as listed in [9]. A first simulation was carried out for low frequency domain

in the range where the characteristics of the ferrite are known. The response, as shown in Fig. 5, is as expected.

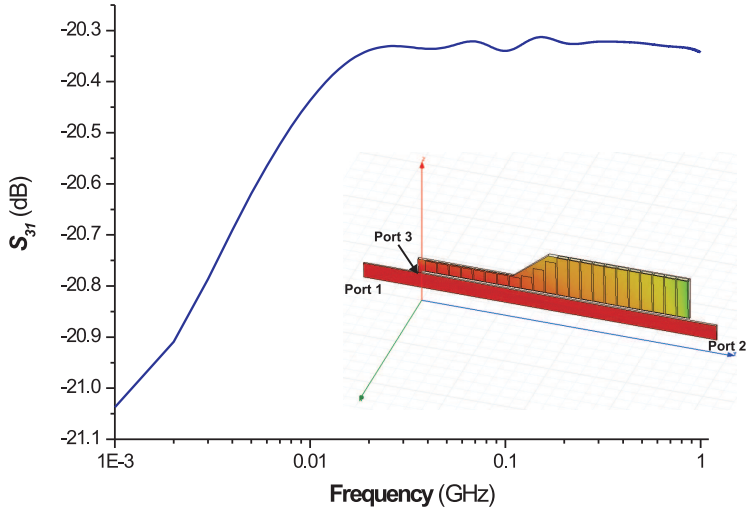

Figure 5: Plot of the low frequency response (S_{31}) of the CTF3 WCM assuming the permeability indicated in [9] for the ferrite.

2.2.2 High frequency

The study of the monitor response at high frequencies is one of the main purposes of the simulations. Figure 6 shows the simulations for different values of permeability μ and magnetic loss tangent δ. The last case (3) represents the same conditions as in case 1, but with the real feedthrough geometry. It is clear that a higher permeability and magnetic loss tangent damps better the waves below 5 GHz. However no resonance around the measured frequency cutoff (6.4 GHz) has been found either with the real or ideal feedthrough. Only the TM_{02} (13.2 GHz) influences the simulations. In comparison with the measurements of the device in frequency domain, Fig. 3, the simulations are quite different. The disagreement could be explained as due to the unknown permeability values of the ferrite at high frequencies, or the construction of the test bench. The construction of a more accurate test bench should clarify these points.

2.3 Wakefields simulation

It is very interesting to simulate the response of the monitor to a stimulus similar to the beam. In this case, the GDFIDL code allows the simulation of the longitudinal impedance and the wakefields. The model is stimulated by a Gaussian line charge of 1 pC. The results and the model used are summed up in Fig. 7. The response of the

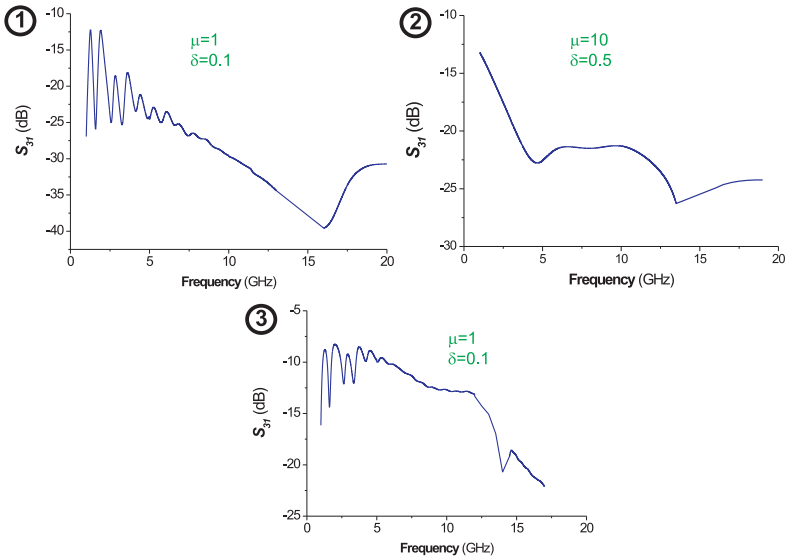

Figure 6: Plot of the high frequency response (S_{31}) of the CTF3 WCM: 1) $\mu = 1$ and $\delta = 0.1$, 2) $\mu = 10$ and $\delta = 0.5$, 3) $\mu = 1$ and $\delta = 0.1$. 1) and 2) describes the behavior with the ideal feedthrough and 3) with the real feedthrough geometry.

monitor is far from being flat but similarities with the test bench measurements (Fig. 3) can be seen. A resonance appears around 13 GHz, which is the cutoff frequency of the TM_{02} mode. It is clear that some modifications to the existing WCM are necessary in order to cover the required 20 GHz bandwidth. The low frequency response of the monitor decays due to the fact that the ferrite was not included in these simulations.

3 New designs for EUROTeV

Within the EUROTeV framework, a new monitor is being designed for measurement of intensity and bunch-to-bunch longitudinal position in future linear colliders (ILC, CLIC). The monitor will be tested in the CLIC Test Facility (CTF3). The beam parameters for those facilities are presented in Tab. 1.
In order to increase the frequency bandwidth for the new Wall Current Monitor (> 20 GHz) different options were studied. The main goal is to increase the high frequency cutoff by improved guiding of the microwaves. In all the cases, the microwaves will have to be damped by some microwave absorbing material as e.g. silicon carbide [10]. The requirements from EUROTeV are presented in Tab. 2.
The three main proposals are shown in Fig. 8. The first version is based on the concept of biconical antennas [11]. The second one is a cylindrical cavity which decreases the gap capacitance and the third proposal is based on intercepting the TEM fields with a coaxial structure which also eliminates the longitudinal gap in the beam pipe. In this

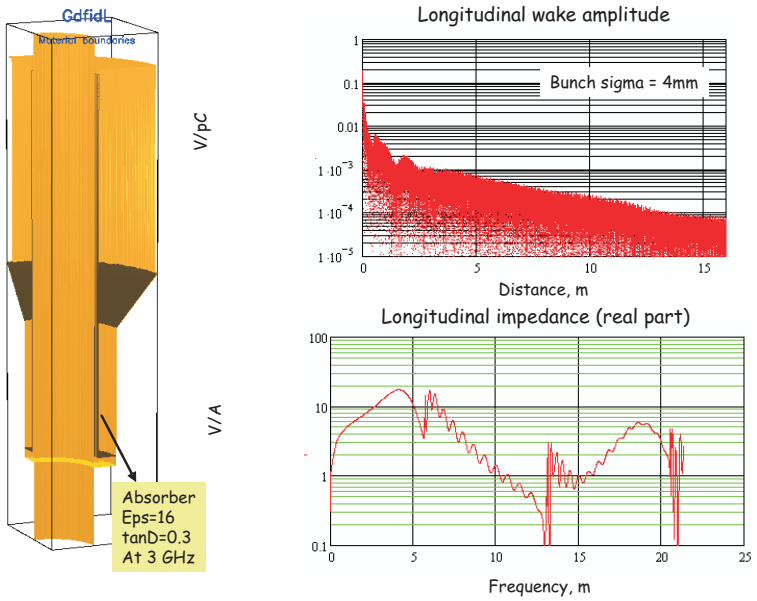

Figure 7: Simulation of the wakefields and longitudinal coupling impedance as function of the frequency of the existing WCM at CTF3.

	CTF3	ATF-2	ILC	CLIC
Energy	184 MeV	1.3 GeV	0.5-1 TeV	0.5-5 TeV
Repetition rate	5-50 Hz	5 Hz	5 Hz	150 Hz
Beam pulse length	140 ns	3 μs	950 μs	58 ns
Bunch spacing	67 ps	300 ns	337 ns	267 ps
Bunch length	1.67 ps	26 ps	1 ps	0.1 ps
Charges per bunch	$1.5 \cdot 10^{10}$	$5 \cdot 10^{9}$	$2 \cdot 10^{10}$	$2.5 \cdot 10^{9}$
Number of bunches	2100	1-20	2820	220
RMS bunch current	1400 A	31 A	3200 A	4000 A
Mean current per pulse	35 A	-	9.5 mA	1.5 A

Table 1: List of the main specifications of the electron beams for the new generation linear colliders.

Frequency bandwidth	100 kHz - $>$ 20 GHz
Bakeout temperature	150°C
Operating temperature	20°C
Vacuum	10^{-9} Torr
Signal transmission	over 10-20m

Table 2: List of the main specifications for the new WCM.

report, only the biconical and coaxial structures are evaluated in detail.

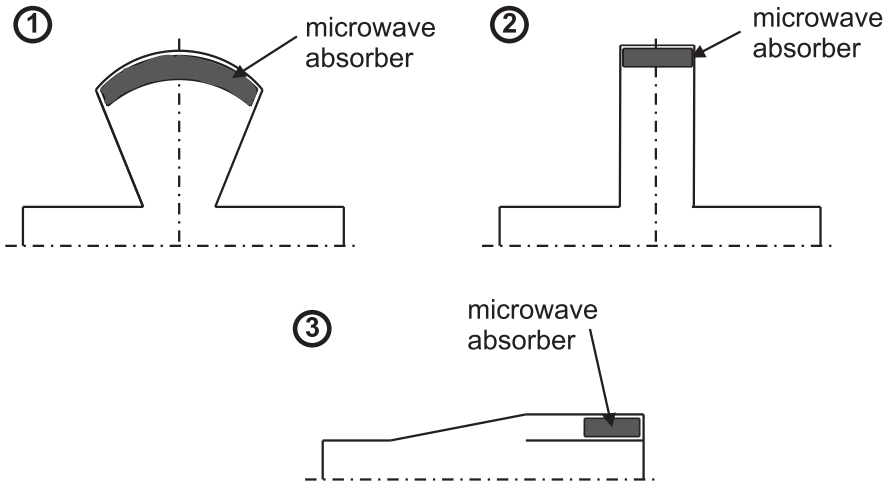

Figure 8: Proposals for extending the bandwidth of the present Wall Current Monitor: 1) biconical antenna, 2) cavity and 3) coaxial structure.

3.1 The biconical structure

In the biconical antenna, the TEM waves are guided away from the gap to the end of the spherical tank, where the microwaves should be absorbed by a combination of silicon carbide and ferrite materials, for high and low frequency waves respectively. Unlike in the old structure, the absence of corners should improve the presence and conversions of HOM in the tank. Hence the bandwidth of such a structure should be wider than in the traditional tank shapes.
The half-angle of the cone ϕ is optimized with the following expression:

$$Z_{cone} = \frac{377}{\pi} \ln\left(\cot\frac{\pi/2 - \phi}{2}\right) \tag{2}$$

where Z_{cone} is the impedance of the cone and ϕ the half-angle of the cone in radians. For a 50 Ω structure with 8 pick-up antennas, the impedance will be distributed around the antennas. Therefore for a conical impedance around 5 Ω, ϕ should be around 2.4°. In order to simplify the manufacturing of such a structure a bigger conical impedance was assumed, giving a $\phi = 20°$.
The feasibility of the structure was simulated using the HFSS code. Figure 9 shows the geometry and ports used for the simulations. If not otherwise specified in the text, Table 3 lists the main parameters of the structure that are used in the simulations. Due to computing limitations and thanks to the radial symmetry only a slice of 3° of the geometry was used in the simulations. From 1 to 20 GHz, the bandwidth was split in different ranges to solve the problem more accurately. In a first set of simulations, the behavior

Beam pipe diameter r_2	40 mm
Coaxial wire diameter r_1	17.4 mm
Length structure L	150 mm
Half aperture angle of the cone ϕ	20°
Gap width e	2 mm
Ferrite relative permeability μ	1
Ferrite loss tangent δ	0.5

Table 3: List of the main parameters used for the simulations of the biconical WCM.

of the structure depending on the parameters of the ferrite was analyzed. In this case, the ferrite fills the conical cavity for simplification. The external radius of the conical cavity was set to 100 mm. The ferrite was simulated for different magnetic parameters: relative permeability $\mu' = 1, 2$ and magnetic loss tangent $\delta = 0.25$ and 0.5. The real behaviour of the ferrite at low frequencies was not included in these simulations, therefore the low frequency part of the response can be someway misleading. The summary of the S parameters results is presented in Fig. 10. S_{21} is the forward transmission parameter along all the structure, S_{11} the reflection and S_{31} the transmission at the gap.
In all the cases the transmission along the structure S_{21} is nearly optimal within the frequency range. However, for S_{11} and S_{31} above 13 GHz there appear some resonances that will be explained later on. For frequencies below this limit, clearly a higher permeability and magnetic loss tangent improve the response of the monitor. Nevertheless, in all the cases S_{31} decreases smoothly whatever the value of the ferrite parameters.
Another set of simulations analyzed the behavior of the monitor for changes in the external radius of the conical cavity. In this case, the cavity was also filled with ferrite with a relative permeability of 1 and a magnetic loss tangent of 0.5. The radius was simulated for values of 50, 75 and 100 mm. The S-parameters obtained in the simulations are compared in Fig. 11. The results shown a better behavior for bigger external radius, but the influence of the radius seems not important once the waves have been properly damped in the ferrite.
An important parameter of the biconical device is the half-aperture radius of the conical cavity ϕ. A variation of the angle implies a change in the impedance of the biconical antenna, as seen in Eq. 2. Some simulations were carried out to study this parameter. The simulations were done with the ferrite filling the conical cavity ($\mu = 1$ and $\delta = 0.5$) and a external radius of the conical cavity of 75 mm. The S-parameters obtained in the simulations are compared in Fig. 12. The results shown a better behavior for a smaller angle (near the calculated value using Eq. 2), but there is no significant differences among them.
A set of simulations was also dedicated to the investigation of the influence of the gap width e on the frequency response of the monitor. Two values $e = 1$ and 2 mm were simulated. A external radius of 50 mm was used. The cavity was filled with ferrite ($\mu = 1$ and $\delta = 0.5$). As shown in Fig. 13, no significant difference between the two versions can be observed.

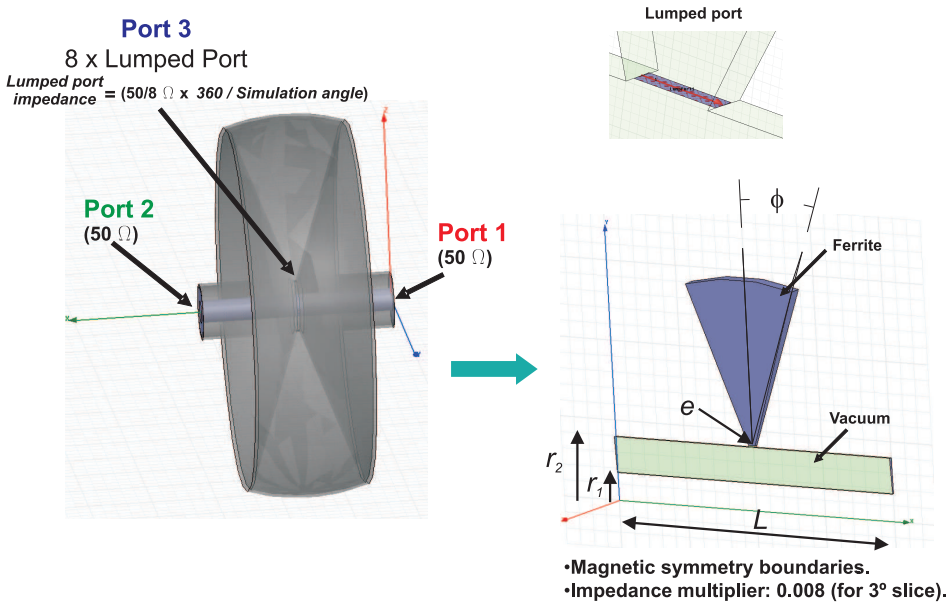

Figure 9: Geometry, ports and boundaries used in the HFSS code for the simulation of the biconical structure. The main parameters are shown: length of the structure L, gap width e, radius of the beam pipe r_2 , radius of the wire used to simulate the beam r_1 and half-aperture angle of the cone ϕ. A lumped port replaces the pick-up antennas.

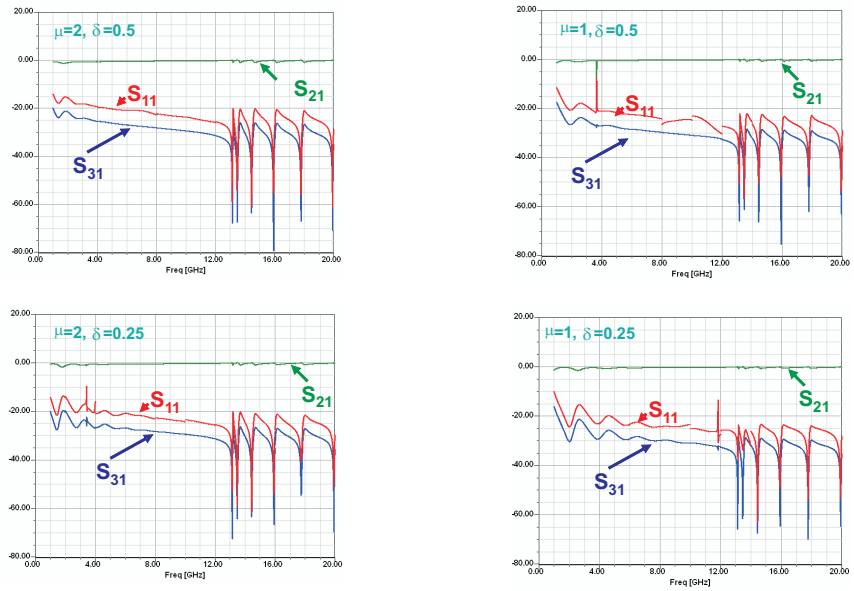

Figure 10: S parameters for the high frequency simulations with the HFSS code for the biconical WCM for different values of relative permeability μ and magnetic loss tangent δ of the ferrite material filling the cavity.

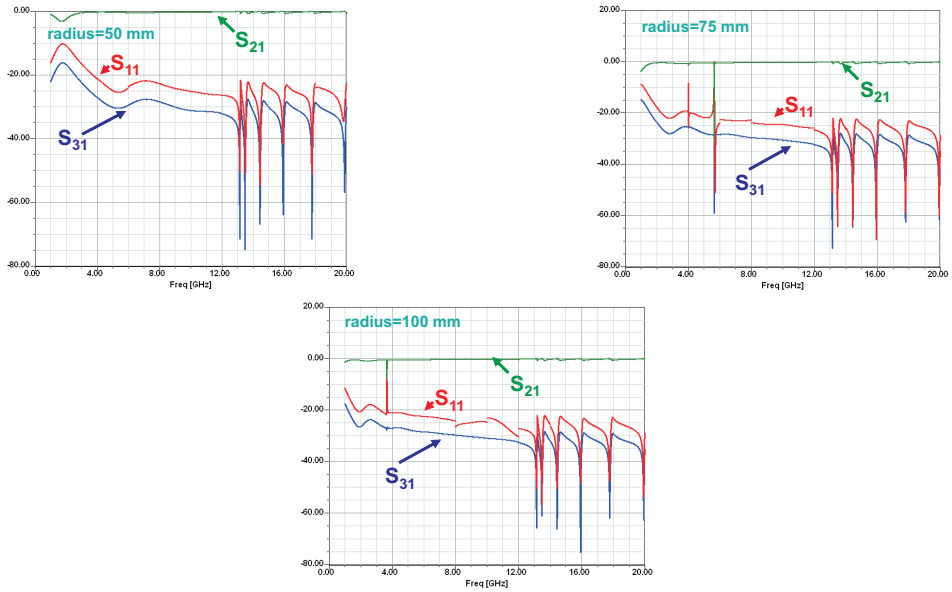

Figure 11: S parameters for the high frequency simulations with the HFSS code for the biconical WCM for different values of the external conical radius.

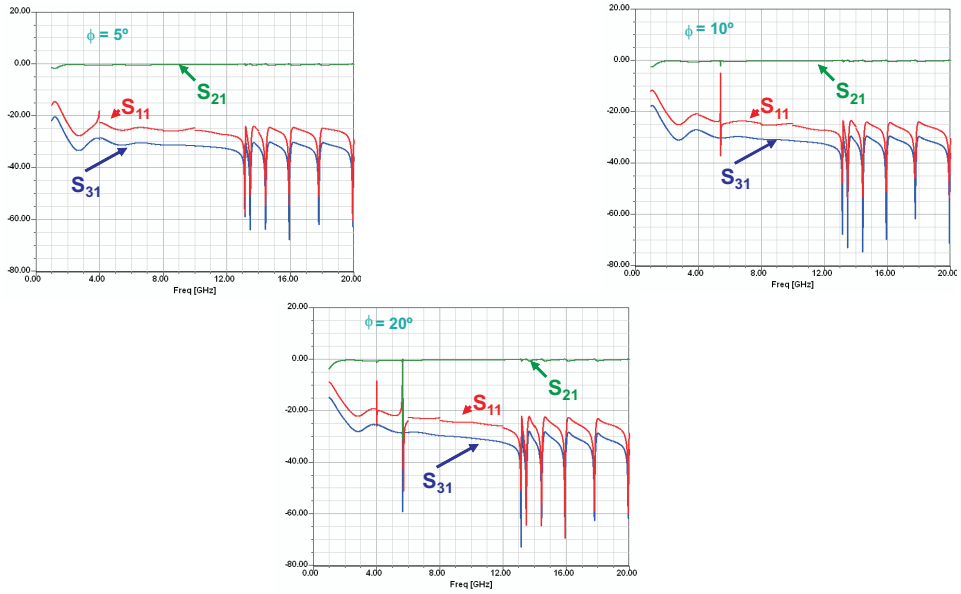

Figure 12: S parameters for the high frequency simulations with the HFSS code for the biconical WCM for different values of the half-aperture angle of the conical cavity ϕ.

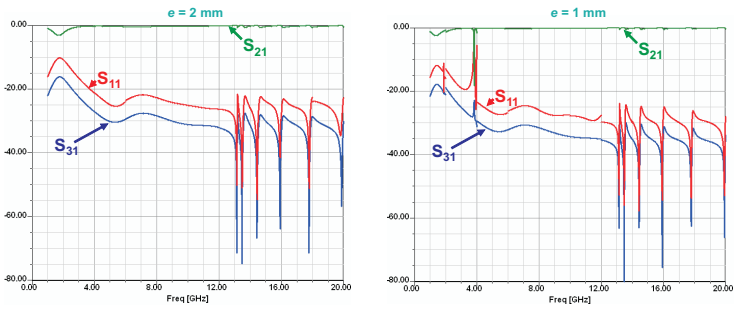

Figure 13: S parameters for the high frequency simulations with the HFSS code for the biconical WCM for different values of gap width e.

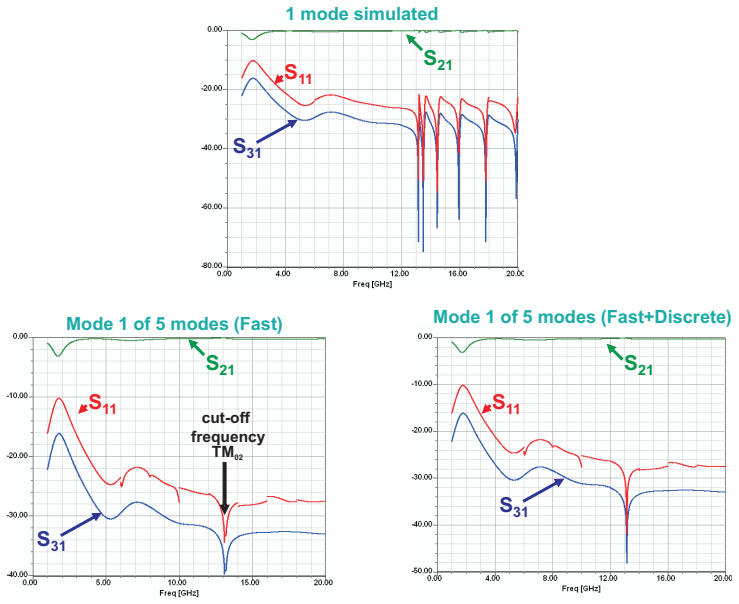

Figure 14: S parameters for the high frequency simulations with the HFSS code for the biconical WCM. In the top case only one mode is simulated. In the bottom left, 5 modes are simulated using a fast sweep. In the bottom right the region of the resonance of the TM_{02} mode is refined using a discrete option for the simulation. The external radius is set to 50 mm.

As mentioned earlier, above 13 GHz, the response of the monitor for S_{11} and S_{31} shows a resonating behaviour. One of the possible reasons of this effect is the appearance of HOM in the structure. These are confined in the volume between Port 1 and Port 2, due to the simulation of one mode only. In fact, for a circular beam pipe of 40 mm diameter the cutoff frequencies for the TM modes corresponds to 5.7 and 13.2 GHz, for the TM_{01} and TM_{02} modes respectively. The cutoff frequency of the TM_{02} corresponds to the first resonant frequency in the simulations. The resonance for the TM_{01} is not so clear although, in some of the simulations, a change in the behaviour of S_{31} can be observed from that frequency. To verify the results, simulations of one mode or five modes are compared in Fig. 14. Results show clearly the improvement in simulating five modes instead of only one. The best result is obtained by applying a fast analysis to the whole range except the part around the cut-off frequency of TM_{02}. The standing waves above the TM_{02} cutoff have been removed. The transmission S_{21} is flat up to 20 GHz.

3.2 Coaxial structures

The coaxial structure is based on intercepting a part of the electromagnetic field generated by the beam. Unlike the existing version, a smooth conical transition avoids the discontinuity and the capacitance across the longitudinal gap is significantly reduced, as proposed in [12]. If the length of the conical transition is reduced to zero, one obtains the classical WCM with a longitudinal gap. The electromagnetic field generated by the beam propagates through the structure consisting of two coaxial tubes in parallel with the beam pipe (see version 3 in Fig. 8). The fields which propagate down the coaxial structure should be completely damped in order to avoid reflections at the downstream end, which is short-circuited. In general, the electromagnetic fields generated by the beam create in the beam pipe an image current of opposite direction and equal magnitude to the beam current. In a coaxial WCM the image current can go through several paths with different impedance:

- an external load (or several symmetrically located around the axis of the beam pipe), generally a resistor, connected to the beam pipe and the inner tube of the coaxial structure through a vacuum feedthrough.
- around all the structure (beam pipe), mainly inductive path.

The current in the required frequency range follows the resistive path (external resistors) and the voltage generated in the resistors is monitored. The use of several resistors symmetrically located around the axis of the beam pipe makes the monitor insensitive to the beam position. The signal monitor is the combination of the signals captured by all the resistors.
The coaxial cavity is terminated by ferrite material which increases the inductance and decreases the low frequency cutoff of the monitor. Using a lumped element approximation, which is only valid up to a certain frequency, the high frequency cutoff is given by the parallel combination of the capacitance of the gap, the load resistors (antennas) and the impedance of the coaxial structure [13].

In most general cases, the signal is picked-up at the starting section of the coaxial line by a miniature wide-bandwidth 50 Ω antenna which is described later. As can be seen in Fig. 15, several modifications to this structure are possible. They all are mainly concerned with the conical transition and the geometry of the coaxial line.

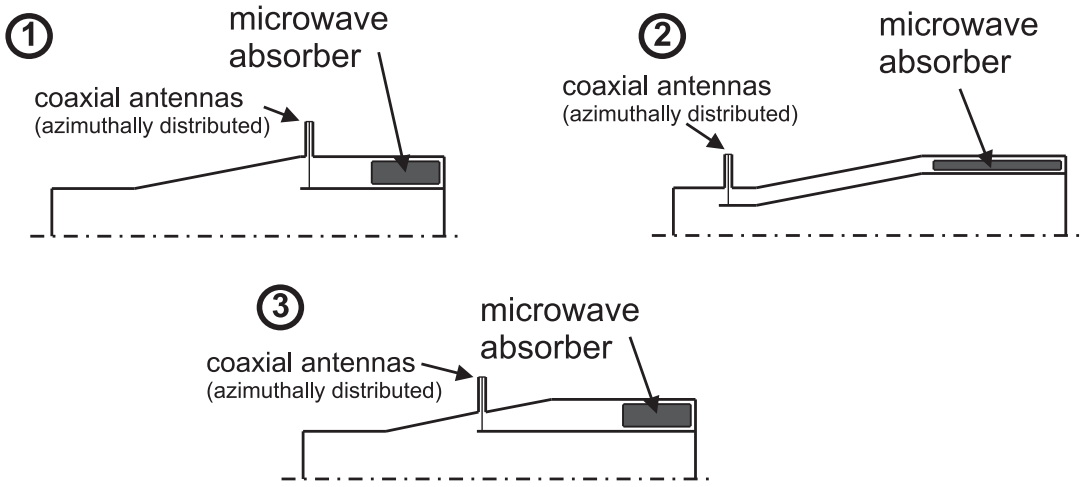

Figure 15: Different versions of the coaxial structure: 1) Coaxial structure starting from the end of the tapering section, 2) Coaxial structure starting before the tapering section, 3) Coaxial structure starting in the middle of the tapering section.

Within the region of the coaxial line, some microwave absorbers will be placed. The proposal is to combine a structure of pyramidal silicon carbide blocks to damp the high frequency components and ferrite material to decrease the low frequency cutoff.

3.2.1 High frequency simulations

Several radiofrequency simulations have been carried out in order to check the performance of these structures. The first step was to test the behaviour using the CST Microwave Studio code.
The transition between the beam pipe of 40 mm diameter and the coaxial structure (taper section) was also analyzed. Figure 16 shows the frequency response of the conical transition for the geometrical parameters of Tab. 4.
The behavior of the coaxial structure was also simulated. Figure 17 shows the frequency response of the coaxial structure for the geometrical parameters of Tab. 5. In the figure, Port 1 or 2 generate the TEM like signal accompanying the beam and S_{21} the transmission from Port 1 to Port 2. Port 4 measures the signal transmitted along the external coaxial structure. The transmission from port 1 is plotted as S_{41}.
The full structure (joining the transition and the coaxial sections) was also simulated. The results are presented in Fig. 18, according to the geometrical parameters in Tab. 6. The transmission from port 1 to port 4 is flat within the required bandwidth, except

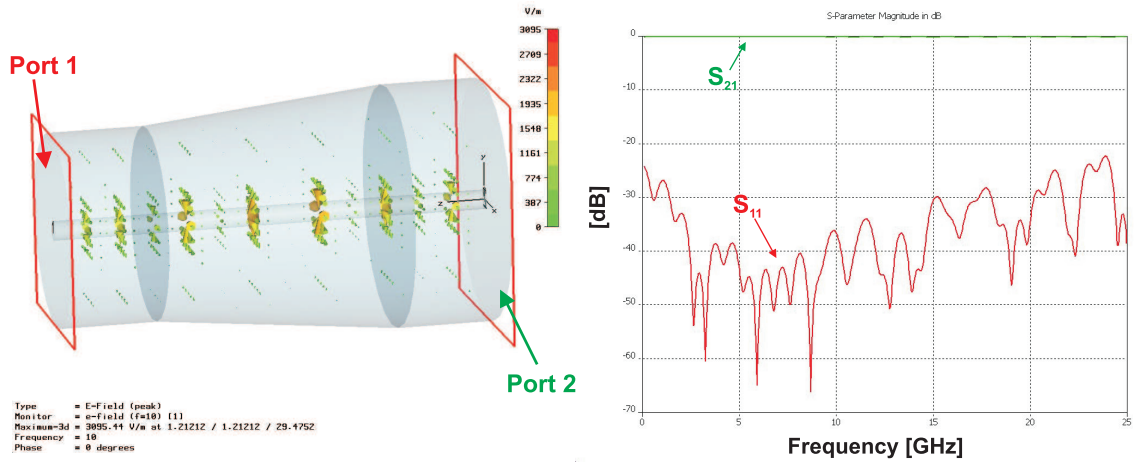

Figure 16: View of the electric field at 10 GHz and the S-parameters for the conical transition. The geometry values are given in Tab. 4.

Length of the straight sections	20 mm
Length of the cone	50 mm
Radius of inner conductor	2 mm
Radius beam pipe	20 mm
Internal radius coaxial structure	25 mm
Thickness internal beam pipe	1 mm

Table 4: Geometrical parameters of the transtion cone of the WCM model used in the simulations.

Total length	40 mm
Length of the coaxial	20 mm
Radius of inner conductor	5 mm
Radius beam pipe	20 mm
Internal radius coaxial structure	25 mm
Thickness internal beam pipe	2 mm

Table 5: Geometrical parameters of the coaxial part of the WCM model used for the simulations.

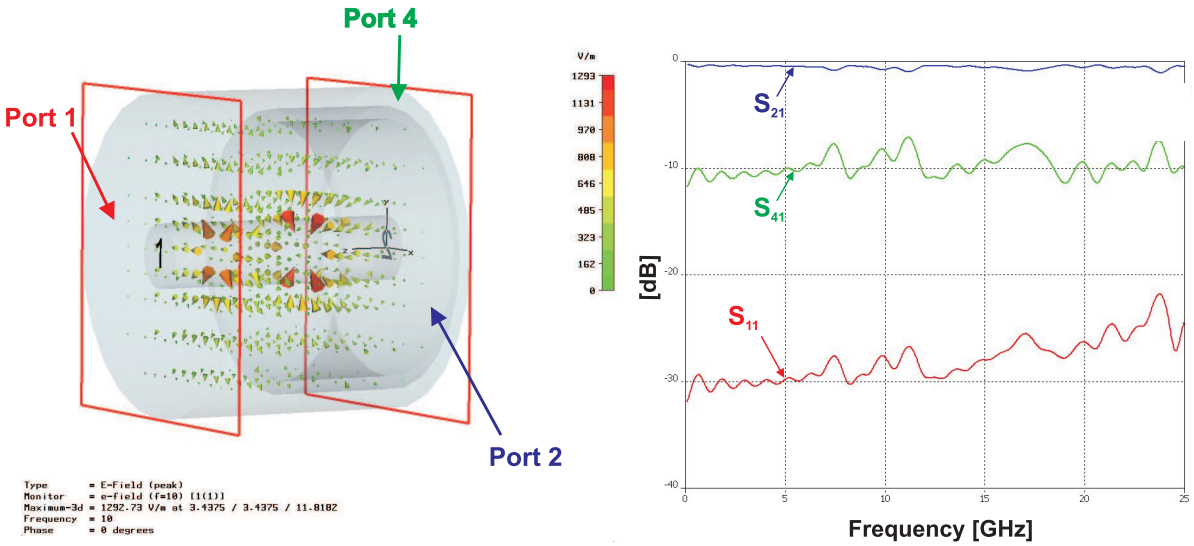

Figure 17: View of the electric field at 10 GHz and the S parameters of the coaxial structure. The geometry values are given in Tab. 5.

some ripples appearing above the cutoff of TM_{01} due to the simulation of only one mode in the ports.

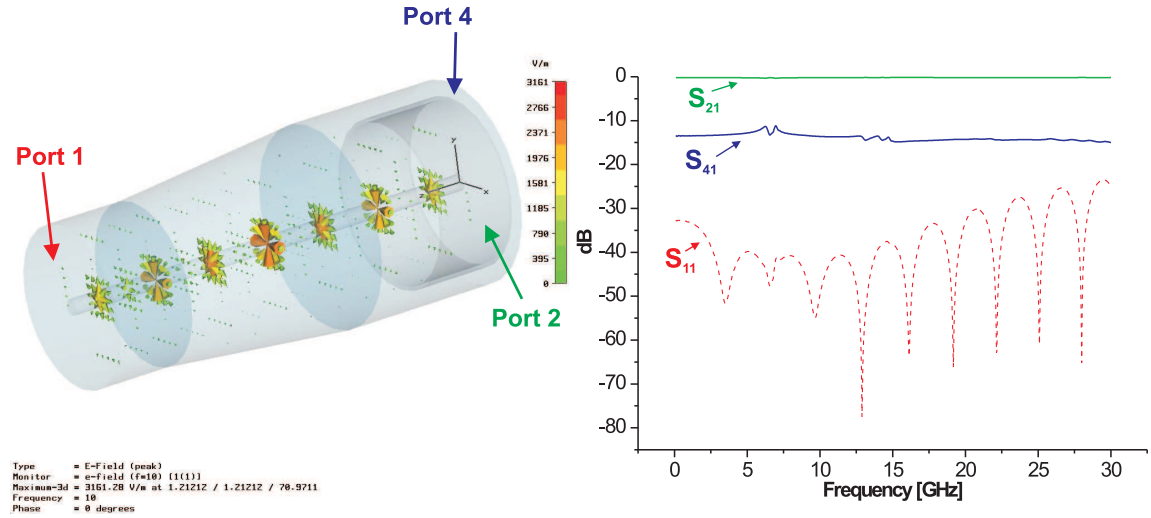

Figure 18: View of the electric field at 25 GHz and the S-parameters for the full model of the coaxial structure. The geometry values are given in Tab. 6.

Finally, four antennas were added to the coaxial structure. In Microwave Studio, it is not easy to implement more than 4 radial ports. To verify what happens qualitatively, the structure can be modeled in a smaller transverse size. The results obtained by reducing

Length straight part (coaxial side)	40 mm
Length straight part (small section)	20 mm
Length conical transition	50 mm
Total length	110 mm
Length of the coaxial	20 mm
Radius of inner conductor	2 mm
Radius beam pipe	20 mm
Internal radius coaxial structure	25 mm
Thickness internal beam pipe	1 mm

Table 6: Geometrical parameters of the full structure WCM model used for the simulations.

the model or increasing the number of antennas are comparable for the same distance between antennas. As it can be seen in Fig. 19, a resonance appears around 25 GHz in the signal picked-up by the antennas (with geometrical parameters as in Tab. 7). The resonance is created by the coupling between the antennas at the frequency when the distance between them equals the wavelength.

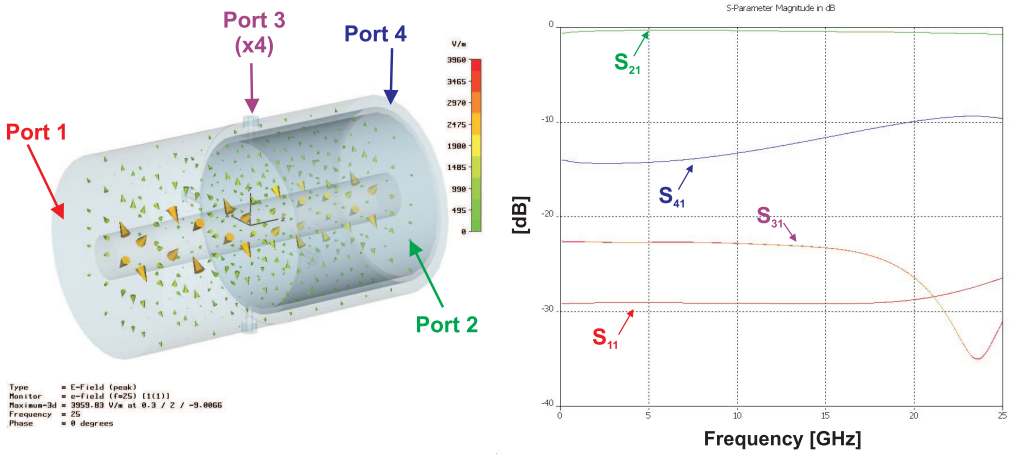

Figure 19: View of the electric field at 25 GHz and the S parameters for the coaxial structure with four antennas. The geometry values are given in Tab. 7.

To complete these results, other simulations were carried out with the Ansoft HSSS code v10.0. Figure 20 shows the frequency response for the full model without antennas, and with 4, 7 and 8 antennas. The dimensions of the model are not the same as in Tab. 7, but the responses agree quite well. It is clear that an increase of the number of antennas improves the high frequency cutoff of the structure. The dependence can be verified by calculating the wavelength of the first resonances with 4, 7 and 8 antennas (around 9 GHz, 15 GHz and 18 GHz respectively) which is 33.3 mm, 20 mm and 16.7 mm, re-

Total length	30 mm
Length of the coaxial	15 mm
Radius of inner conductor	2 mm
Internal radius beam pipe	8 mm
Thickness beam pipe	1 mm
Feedthrough inner diameter	1.4 mm
Feedthrough outer diameter	0.6 mm

Table 7: Geometrical parameters of the coaxial part of the WCM model with four feedthroughs used for the simulations.

spectively. The wavelengths match with the arc distance between the antennas in each case.

Due to the big computer requirements of the simulations of the full model, only a slice of the model was simulated. The feedthrough is cut in two-halves by the slice, and the second symmetry wall corresponds to the half-distance between two feedthroughs in the case where 16 feedthroughs are used, the angle of the slice corresponds to 11.25°. In this case, four modes are simulated in Ports 1 and 2 to remove some of the standing waves observed in the previous simulations. In addition, the radius of the wire has been reduced to 0.1 mm. The results are shown in Fig. 21. As expected, the resonance frequency from the feedthroughs was increased by doubling the number of feedthroughs to 16. The level of the Port 3 and 4 signals have decreased due to the reduction of the wire diameter. Some resonances around 6 GHz and 13 GHz are now visible, which correspond to TM_{01} and TM_{02} modes of the circular beam pipe (20 mm radius). The multiplication of peaks around these frequencies are believed to be caused by standing waves in the conical transition. A more detailed simulation of different tapering lengths is given in [12].

3.2.2 Wakefields and longitudinal impedance

The beam coupling impedance and the wakefields for variations of the geometry of the coaxial structure were simulated using GDFIDL and compared with the results obtained for the existing monitor. The model is stimulated by a gaussian line charge of 1 pC. The standard deviation of the stimulus is 1.66 mm. The versions 2 and 3 (see Fig. 15) of the coaxial structure are simulated and compared in Fig. 22. The version 3, or external coaxial WCM, has a very flat response within the required frequency range and it could be a very interesting solution.

The next step was to compare the performance of version 1 and 3 with 16 antennas (see Fig. 15). Figures 23 and 24 shows the simulation of the longitudinal impedance and the wakefield for two variations of the coaxial model with 16 antennas. In Fig. 23 (version 3 of Fig. 15)), the coaxial part starts in the middle of the conical part. In Fig. 24 (version 1), the coaxial part starts after the conical transition. Even if the response is very similar for both structures, the latter (version 1) seems to provide a more flat

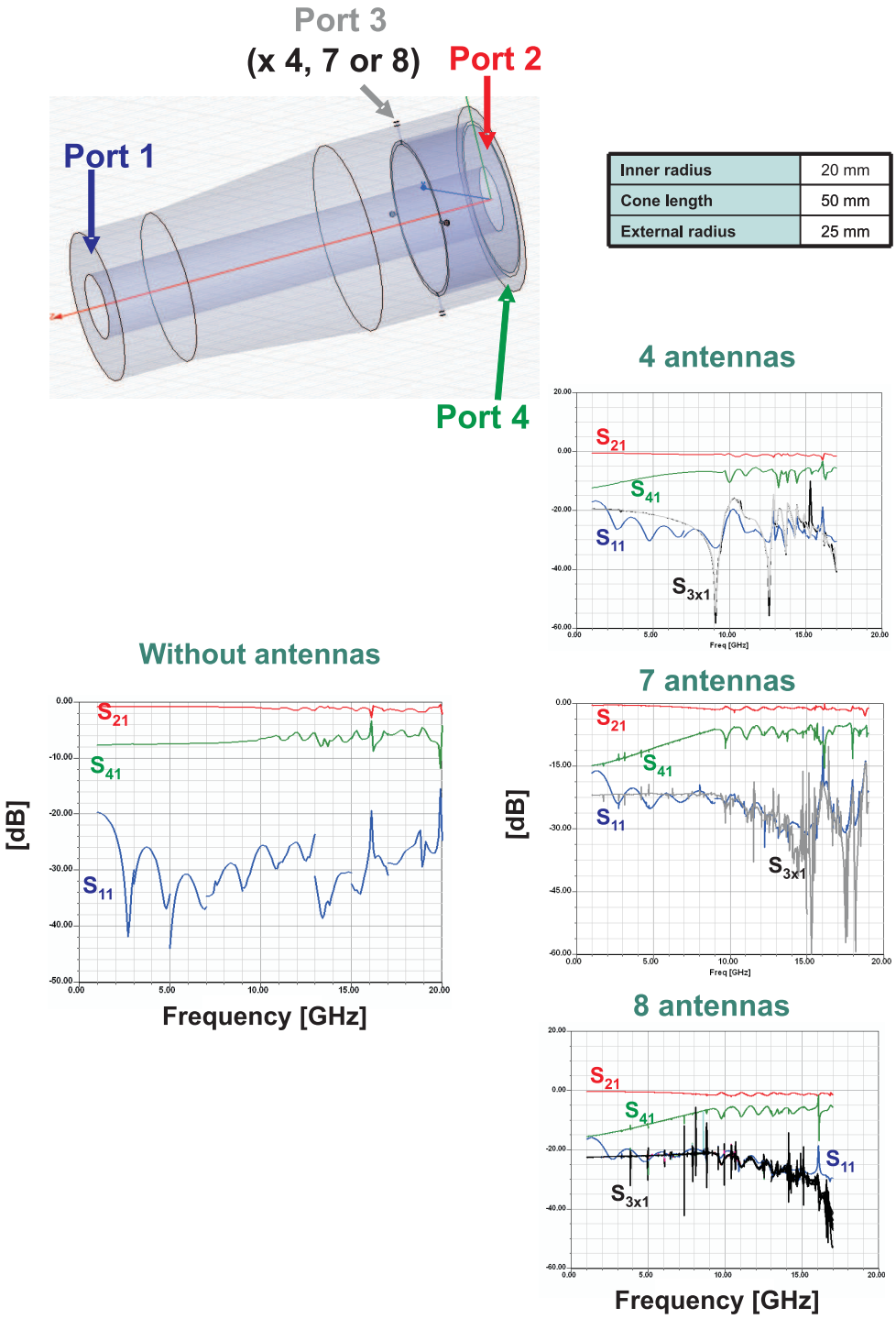

Figure 20: S parameters for the coaxial structure simulated using the HFSS code. Different simulations with no antennas, four antennas or eight antennas are given.

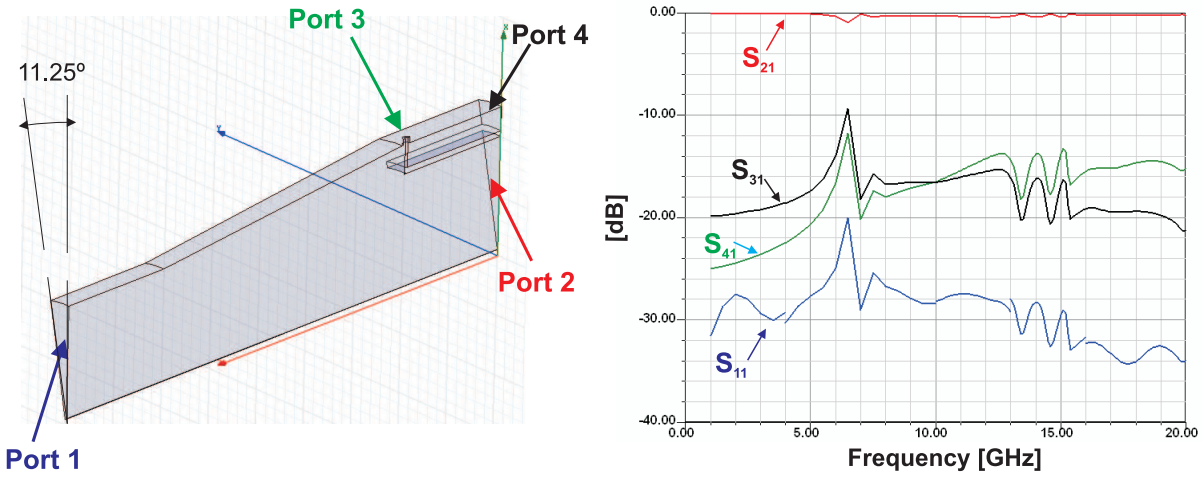

Figure 21: S parameters for a slice of the coaxial structure simulated using the HFSS code. Four modes are simulated in Port 1 and 2.

longitudinal impedance and lower levels of wakefields.

3.2.3 First mechanical proposal

A first draft of the mechanical design of the coaxial structure with 16 antennas is shown in Fig. 25. The design simplifies the construction by introducing modifications of the present design. The quantity of pieces to be modified is minimized. For example, some pieces like the ferrite rings could be recovered from the existing wall current monitors.

4 The miniature feedthrough

The very small feedthrough used in the present version of the WCM was initially developed for the pacemaker market, but due to its very small size it is very good for microwave applications as well (Fig. 26).
The feedthrough was optimized [7] for high frequency response by modifying the air side central pin to fit with a Radiall K 46 GHz SMA connector. Also a better adaptation to 50 Ohm was obtained over 1.4 mm, by welding a titanium tube to the existing titanium part (see Fig. 27). As can be seen, the effect of the tube and the small region of air gives an impedance over half of the length which is very close to 50 Ω.
The feedthrough has been measured with a network analyzer and it has been found that the insertion loss is 0.3 dB at 10 GHz and 1.9 dB at 19 GHz. Time domain measurements indicate a 3 dB bandwidth of 25 GHz.
HFSS simulations have confirmed the good electrical performance of this feedthrough. In Fig. 28 almost no insertion loss is observed up to 20 GHz (around 1 dB at 20 GHz), which is in good agreement with the measurements.

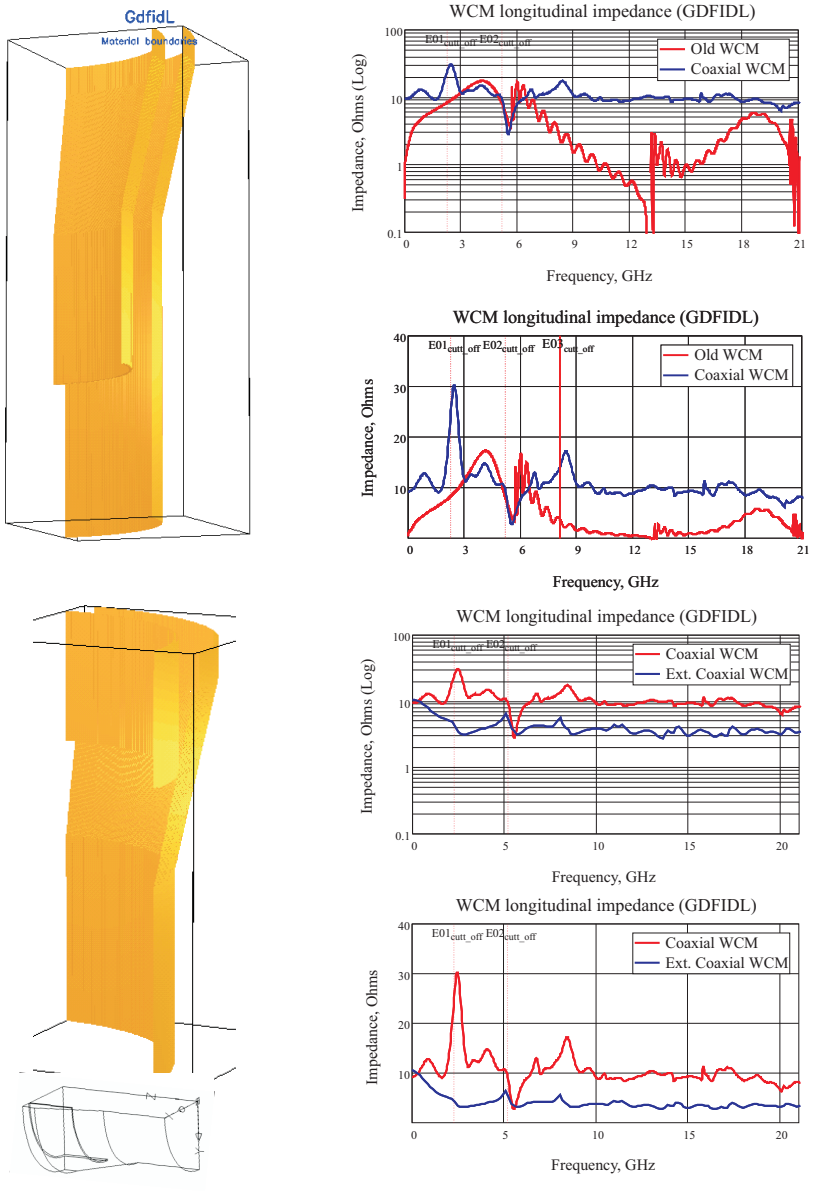

Figure 22: Plot of the simulations of the wakefields and longitudinal impedance for two types of coaxial structures.

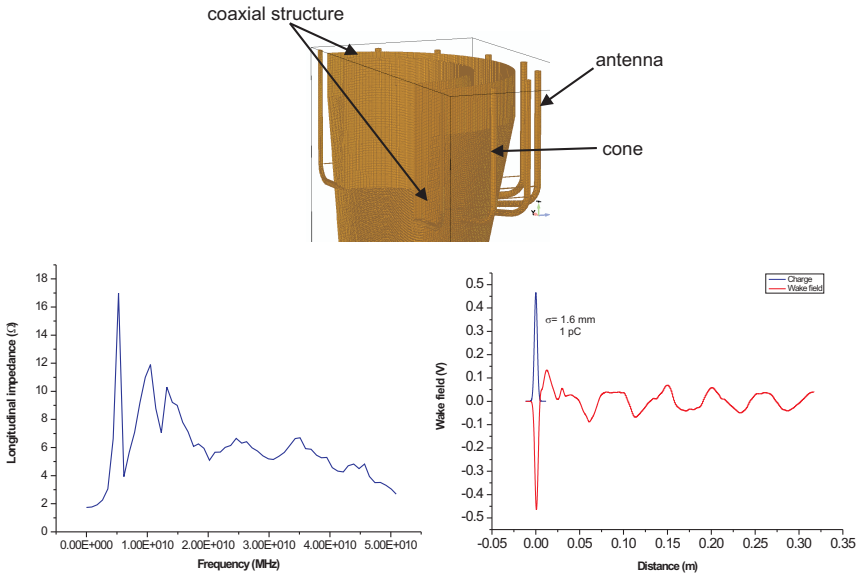

Figure 23: Plot of the wakefield and the longitudinal impedance simulated in GDFIDL for a coaxial structure with 16 antennas entering into the transition.

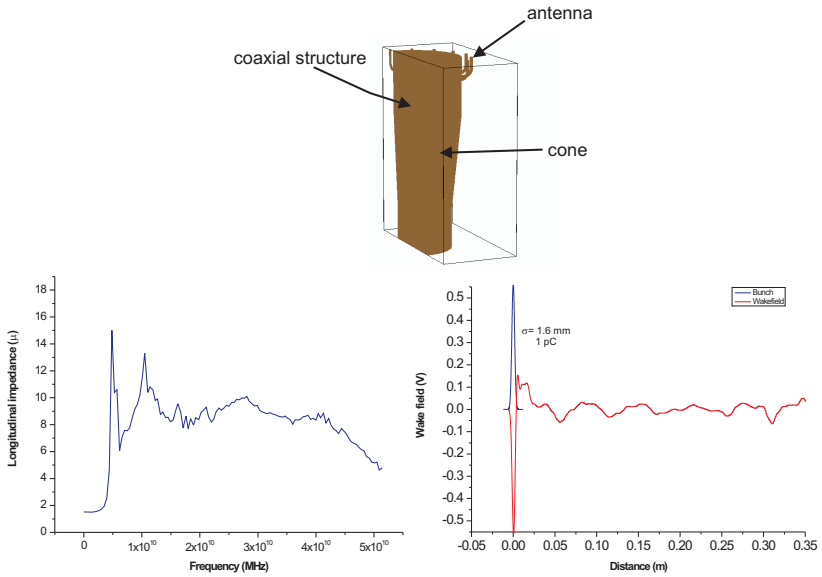

Figure 24: Plot of the wakefield and the longitudinal impedance simulated in GDFIDL for a coaxial structure with 16 antennas after the transition.

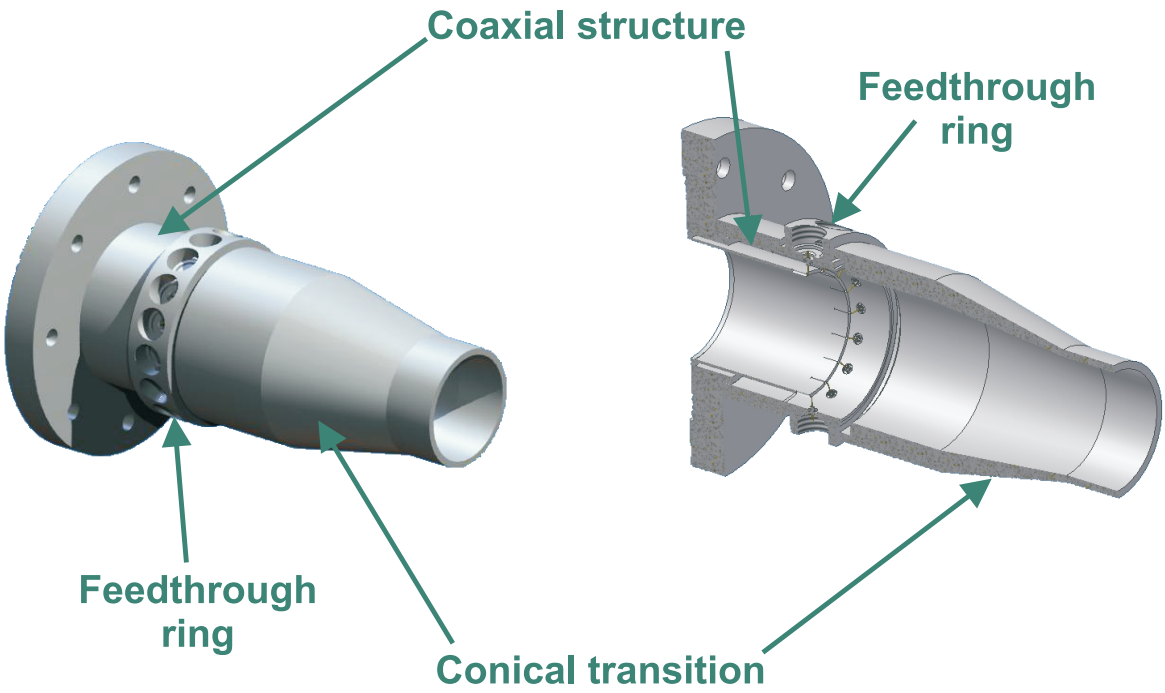

Figure 25: Draft of the mechanical 3D model (left) and section (right) of the vacuum chamber and components of the design proposed for the new WCM.

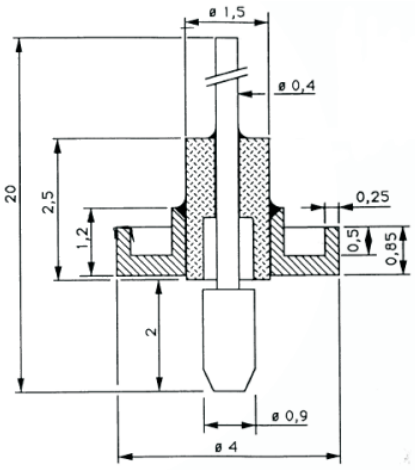

Figure 26: Feedthrough schematic with modification for 46 GHz SMA connector (enlarged 0.9 mm pin).

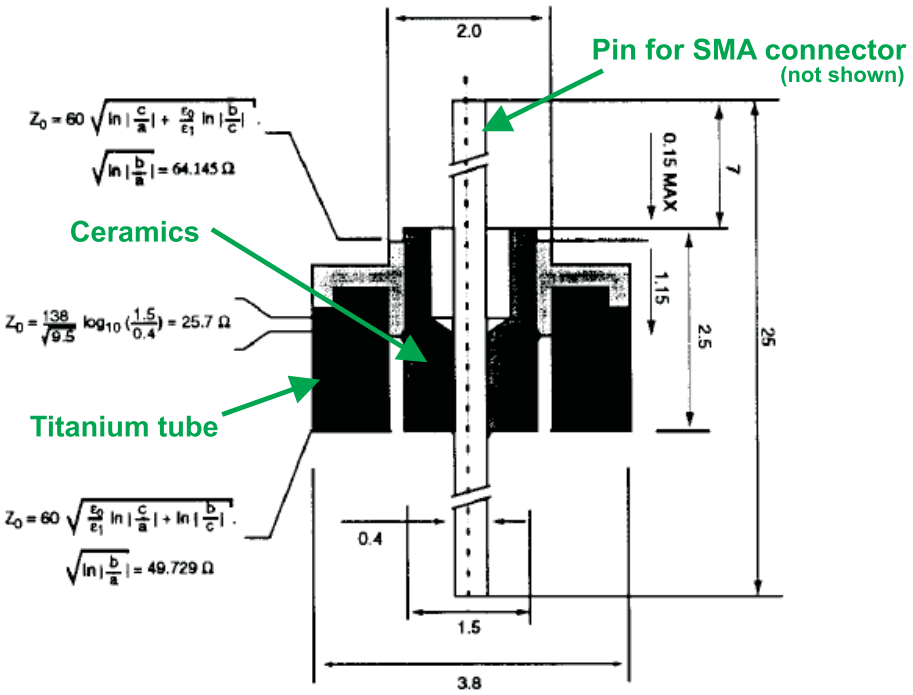

Figure 27: Feedthrough with added tube for matching to 50 Ω

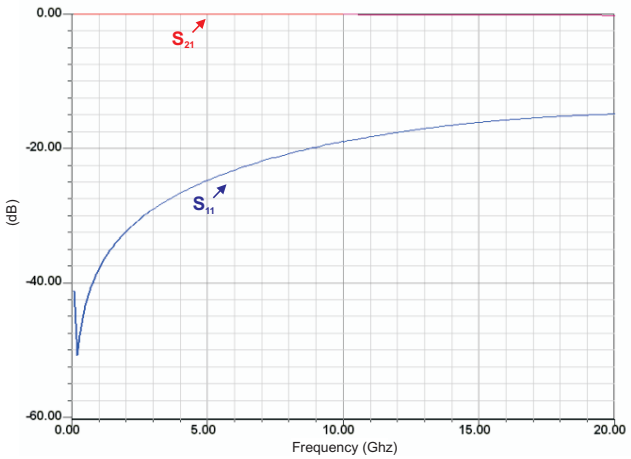

Figure 28: Simulation of the insertion loss (S_{21}) and reflection (S_{11}).

The feedthrough is bakeable up to 150°C and vacuum tight down to 10^{-9} Torr. In the latest batch several feedthroughs have been found leaking after electron beam welding and/or baking at 150°C. It is at present not well understood if the feedthroughs develop a leak due to heating from the welding or from the bake out. In the present WCM design the feedthroughs are welded into the WCM tank and changing them is therefore quite complicated.
A study to weld the feedthrough into a dismountable DN16 flange (or smaller) has started and this is what we expect to use for the new WCM.

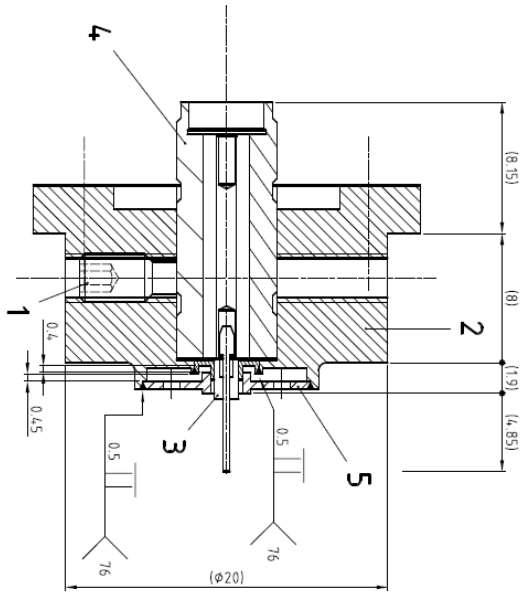

Figure 29: Feedthrough welded into DN16 flange

It is also important to understand the reason why some feedthroughs develop leaks either during welding or during bake out. For this, a batch of $\sim$ 100 pieces will be vacuum tested, submitted to several temperature cycles, and then tested again. If the feedthroughs are still good the mechanical stresses during welding must be understood and corrected. A drawing of the miniature feedthrough mounted in an CF DN16 flange can be seen in Fig. 29.

5 Signal transmission and observation

The transmission and posterior analysis of a signal with frequency components up to 20 GHz is a challenging task that requires a careful analysis of several possibilities. In the future system, the signal picked-up by the WCM has to be transmitted before analysis over path that could go up to 10 or 20 m.
For the transmission, coaxial cables are not a good option due to the signal losses and the propagation of HOM's at high frequencies. Optical links represents the most suitable option because of the low attenuation with length. To match the requirements, it is

foreseen to install a commercial fiber optic link with a bandwidth from 100 MHz up to 18 GHz [14]. Due to the high low frequency cutoff, the possibility of transmitting the low frequency signal components by a coaxial cable should be studied.
There are also several options for the monitoring of the signal. Sampling oscilloscopes are not easy to implement due to the requirements of trigger and beam stability. On the other hand, real-time oscilloscopes are limited in bandwidth. Some models with a bandwidth up to 18 GHz can be found in the market. The problem is the cost of these devices which starts from 115000 US$ for a 13 GHz model.

6 Conclusions and outlook

Several new options to improve the performance of the existing WCM at CTF3 have been reported. After evaluation and discussion of the simulations, the main conclusions are:

- The coaxial structure is the best candidate, since it shows the best high frequency performances. Furthermore, only small modifications of the present design are required instead of a total re-design. Mechanical changes are minimized.
- To create a smooth conical transition before the coaxial part. That implies the reduction of the capacitance of the gap and the presence of HOM's.
- To add microwave absorbers before the low frequency absorbers (ferrite rings) within the cavity created by the coaxial part and the vacuum tank. Pyramidal pieces of silicon carbide will be tested as RF absorbers.
- To test completely the assembly process of the RF feedthroughs.
- To verify the feasibility of increasing the number of antennas (feedthroughs) to 16 instead of 8

From now on, the intention is to continue the design of the proposed solution, design a prototype, construct and test it. The main topics to be studied are:

- The implementation of real microwave absorbers in the simulations in order to develop the 3D design.
- The construction of an improved test bench.
- The study of the signal transmission from the WCM to the acquisition system.

Acknowledgement

This work is supported by the Commission of the European Communities under the 6^{th} Framework Programme "Structuring the European Research Area", contract number RIDS-011899.

References

[1] M. Battaglia, A. de Roeck, J. R. Ellis, and D. Schulte. *Physics at the CLIC Multi-TeV Linear Collider : report of the CLIC Physics Working Group*, volume CERN-2004-005. CERN, 2004.

[2] P. Odier. A new wide band wall current monitor. In *6th European Workshop on Beam Diagnostics and Instrumentation for Particle Accelerators DIPAC 2003*, page 216, May 2003.

[3] J. Durand, T. Tardy, and M. Wurgel. A 10 GHz wall current monitor. *CERN-PS-LP-Note-95-09 (Tech.)*, 1995.

[4] K. Satoh. New wall current beam position monitor. *IEEE Trans. N. Sci.*, NS-26(3):3364–3366, 1979.

[5] G. C. Schneider. A 1.5 GHz wide-band beam-position-and-intensity monitor for the electron-positron accumulator (EPA). *CERN-PS-97-A-BT*, 1987.

[6] R. Bossart. Microwave beam position monitor using a re-entrant coaxial cavity. *CERN-PS-91-59-LP*, 1992.

[7] J. Durand, T. Tardy, and R. Trabelsi. A miniature ultrahigh vacuum feedthrough usable from DC to 20 ghz. *CERN-PS-LP-Note-96-09 (Tech.)*, 1996.

[8] F. Caspers. Impedance determination from bench measurements. *CERN-PS/2000-004(RF)*, 2000.

[9] Fair-Rite website. http://www.fair-rite.com.

[10] M. Luong, I. Wilson, and W. Wuensch. RF loads for the CLIC multibunch structure. *CERN-PS-99-020-LP*, 1999.

[11] G. Liu and C. A. Grimes. Spherical-coordinate FDTD analysis of conical antennas mounted above finite ground planes. *Microwave and Optical Technology letters*, 23.

[12] T. Kroyer. A structure for a wide band wall current monitor. *CERN-AB-Note-2006 RF*, 2006.

[13] T. Linnecar. The high frequency longitudinal and transverse pick-ups used in the SPS. *CERN-SPS-ARF-78-17*, 1978.

[14] MITEQ. http://www.miteq.com/micro/fiberoptics/index.html.